A Continuum Model for Polymer Adsorption at the Solid−Liquid Interface

Vinay A. Juvekar,* Chengara V. Anoop, and Sudip K. Pattanayek

Department of Chemical Engineering, Indian Institute of Technology, Powai, Mumbai - 400 076, India

Vijay M. Naik

Unilever Research India, 64 Main Road, Whitefield, Bangalore 560 066 India

Received May 12, 1998; Revised Manuscript Received September 16, 1998

ABSTRACT: A continuum version of self-consistent field model for polymer adsorption at the solid−liquid interface has been formulated and solved to obtain configurational statistics of an adsorbed polymer chain. The solid surface is viewed as a singular phase (having zero thickness but finite adsorption capacity) in equilibrium with the solution. Chain configuration is described by the random flight model. The surface boundary condition accounts for both the configurational constraint and the adsorption equilibrium. The potential field is described by a modified form of the Flory−Huggins theory, which incorporates the effect of unequal partial volumes of the species (chain segment and solvent molecule) in the solution and their unequal partial areas in the surface phase. The model predictions are in qualitative agreement with the Scheutjens and Fleer model, except that the model predicts a negative value of χ_c^*, the critical adsorption energy parameter. The model has been validated using experimental data reported in the literature. The present model has advantages over the Scheutjens and Fleer model both in terms of ease of computation and the ability of the model to account for the difference in the packing densities between the solution and the surface.

Introduction

Self-consistent field (SCF) models[1−5] have been applied to predict characteristics of polymer adsorption at interfaces. In these models, the statistical distribution of equilibrium configurations of a polymer chain in the interfacial region is assumed to be governed by a potential field which simulates the effect of environment in which the test chain is present. This potential field (termed self-consistent field) is, in turn, determined from the statistically averaged composition profile based on the above distribution. In an idealized picture, the configuration of a real polymer molecule in the interfacial region is modeled as a random walk path of a statistical segment. The two important parameters in continuum models, viz. the number of statistical segments per polymer chain (r) and the length of each segment (l), can be determined by matching both the extended contour length and the radius of gyration of the real and the idealized flexible chains. This procedure provides a physically meaningful connection between the model parameters and stiffness of the real polymer molecule. Their counterparts in the lattice theory, namely the lattice spacing and the lattice coordination number, have some limitations. First, they have often been used as adjustable parameters. Second, in a multicomponent system, a single set of lattice parameters is required to characterize all species. These limitations of the lattice models lead to an inaccurate estimation of the system entropy, a drawback not present in the continuum models. Another advantage of a continuum approach is that it can account for externally imposed/internally generated potential fields in a straight forward manner. For example, while the continuum models can describe the electric field in ionic system using the Poisson equation, the lattice models necessitate a coarser approach of dividing the interfacial region into a series of Stern layers.[6] Another drawback of a lattice-based model is that the number of finite difference equations describing the configurational distribution of a chain is proportional to the number of segments of the chain. As a result, the computational load increases roughly quadratically with the chain length.[2] On the other hand, in continuum models, the number of segments in the chain appears as a parameter, making computational intensiveness independent of the chain length.

Despite these advantages, continuum models for polymer adsorption have not been solved rigorously for solid−liquid interfaces. The difficulty lies in correctly accounting for the effect of an impenetrable surface on the configuration of a chain in its vicinity. A correct boundary condition must reflect the fact that if a segment is attached to the surface**,** the probability of finding its immediate neighbors near the surface is much higher due to the connected nature of segments. The problem is compounded by the steep profile of the potential generated by the surface. A frequently used solution procedure assumes that the spatial distribution of a polymer segment is independent of its position along the contour length of the chain (infinite chain approximation).[7−9] This approximation not only obviates the necessity to incorporate the connectivity constraint at the solid boundary but also facilitates the transformation of the effect of the surface potential into a boundary condition for the segmental probability. An obvious consequence of this simplification is that although these models yield the volume fraction profile for polymeric species, they fail to provide information about the segmental probability distribution. Attempts have been made to incorporate corrections to account for the finite length of chain.[10,11] However these approaches are

* To whom correspondence should be addressed. E-mail: vaj@che.iitb.ernet.in.

10.1021/ma980760i CCC: $18.00
Published on Web 01/21/1999

approximate in nature.

An alternative approach is to view the surface as a separate phase, composed of polymer and solvent, in equilibrium with the solution phase. Ploehn et al.[5] and Ploehn and Russell[12] have used this approach. However, to account for the configurational constraint imposed by the surface, they modify the connectivity equation to make it applicable for distances less than a segment length from the surface. They derive a surface boundary condition by dropping the second-order derivative of segmental probability from the modified connectivity equation. This last step is arbitrary and cannot be mathematically justified. It is impossible to impose a boundary condition on an equation which already incorporates the effect of the boundary. Such an equation necessarily breaks down at the boundary.

In the present work, we have also employed the concept of surface phase. However, our approach differs from that of Ploehn et al.[5] in that the connectivity constraint imposed by the surface is accounted for solely by a boundary condition on segmental probability. The model equations are rigorously solved to obtain segmental distribution profile, from which the other characteristics of the adsorbed layer are derived. The salient predictions of our model have been compared with those of the lattice model of Scheutjens and Fleer[2] in order to bring out the similarities and differences between them. The model has been validated using experimental data reported in the literature.

Model Development

Consider a solution comprising of a single, unchanged and monodisperse polymer species, having r statistical segments, each of length l and a monomeric solvent species, in contact with a plane, homogeneous solid surface of infinite dimensions. The surface is located in the $x-y$ plane ($z = 0$) with the positive z direction pointing into the solution. Species (segment or solvent) located at $z = 0$ can be either in the bound state (i.e., under the influence of the surface potential) or the unbound state. Equilibrium between the bound and unbound states is assumed. The surface phase, which comprises the bound species, is assumed to have zero thickness but a finite capacity to hold mass.

We use here a heuristic approach[5] to derive the random flight model. The polymer connectivity in the region $z > l$ can be expressed as (see Figure 1a)

$$G_p(z,q) = G_{p,f}(z)\left[\frac{1}{4\pi l^2}\int_{S_s} G_p(z_s, q-l)\, dS_s\right] \qquad (1)$$

In this equation, subscript p refers to the polymer species. The term $G_p(z,q)$ denotes the probability weight of the end segment of the chain of length q to lie at z while $G_{p,f}(z)$ is the corresponding probability weight of an unconnected (free) segment. All probability weights have been obtained by normalizing the probabilities with respect to the corresponding values in the bulk solution (located at $z = \infty$). S_s denotes the surface of the sphere of radius l, centered at z.

Expanding the integrand in eq 1 in Taylor series about the point (z, q) and retaining the lowest order nonzero terms in the expansion, we get the following expression.

$$l\frac{\partial G_p(z,q)}{\partial q} = \frac{l^2}{6}\frac{\partial^2 G_p(z,q)}{\partial z^2} + \left[1 - \frac{1}{G_{p,f}(z)}\right]G_p(z,q) \qquad (2)$$

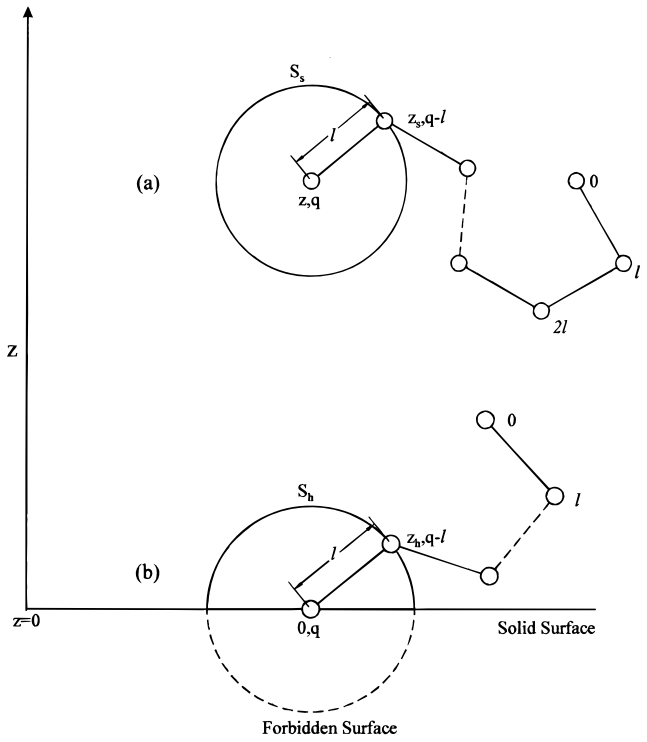

Figure 1. Schematic representation of a polymer chain of length q, the end segment of which is placed at (a) $z > l$ and (b) $z = 0$.

The truncation of the Taylor series in eq 2 is valid only if the order of magnitude of l is lower than those of q and z. The order of magnitude of q is equal to the chain length (rl), while that of z equals the thickness of the adsorbed layer, which, in turn, can be equated to the order of magnitude of the radius of gyration of the chain ($\sqrt{r}l$). Hence eq 2 is valid only if the chain is long ($r \gg 1$).

$G_{p,f}(z)$ is determined by the Boltzmann equation

$$G_{p,f}(z) = e^{-u_p(z)/kT} \qquad (3)$$

where $u_p(z)$ is the potential of a free polymer segment at location z, with reference to the bulk solution which is used as the datum.

We note that for a small value of u_p ($u_p \ll kT$), eq 2 reduces to the standard form of the random flight equation, which can be deduced on the basis of statistical mechanics.[13]

The initial condition for q in eq 2 can be obtained by noting that the free segment is also an end segment of a chain of zero contour length, i.e.,

$$G_p(z,0) = G_{p,f}(z) \qquad (4)$$

The boundary condition of eq 2 corresponding to the bulk solution is

$$G_p(\infty,q) = 1 \qquad (5)$$

The boundary condition at $z = 0$ is derived with the help of Figure 1b as follows. If the end segment of a chain of length q is at $z = 0$, the penultimate segment can be located either on the surface of hemisphere of radius l centered at $z = 0$ or in the surface phase. This

condition, for the end segments in unbound and bound states, can be expressed by eqs 6 and 7, respectively.

$$G_p(0,q) = G_{p,f}(0)\left[\frac{1}{4\pi l^2}\int_{S_h} G_p(z_h, q-l)\, dS_h + G_p^*(q-l)\right] \quad (6)$$

$$G_p^*(q) = G_{p,f}^*\left[\frac{1}{4\pi l^2}\int_{S_h} G_p(z_h, q-l)\, dS_h + G_p^*(q-l)\right] \quad (7)$$

Here, $G_{p,f}^*$ represents the probability weight of a free segment to lie in the surface phase and can be written as

$$G_{p,f}^* = e^{-u^*_p/kT} \quad (8)$$

where u_p^* is the potential of a free polymer segment in the surface phase. $G_p^*(q)$ represents the probability weight of the end segment of a chain of length q to lie in the surface phase.

The factor used for normalizing the integral terms of eqs 6 and 7 is $4\pi l^2$ (the area of a sphere of radius l) because the integration is actually performed over the entire spherical surface (including the dotted surface in Figure 1b). However, since the segment is not allowed to cross the solid surface, the probability of the penultimate segment to lie on the dotted surface is zero, and hence only the upper part of the surface integral needs to be considered. The configurational entropy loss suffered by the chain due to the presence of the solid surface is thus accounted for.

Comparing eqs 6 and 7 we get

$$\frac{G_p^*(q)}{G_p(0,q)} = \frac{G_{p,f}^*}{G_{p,f}(0)} = e^{-[u^*_p - u_p(0)]/kT} \quad (9)$$

where the third term is derived using eqs 3 and 8. Equation 9 expresses the equilibrium relationship between the bound and unbound states at $z = 0$.

Equation 6 can be converted to the differential form by a Taylor series expansion of $G_p(z_h, q-l)$ about $(0,q)$, and expansion of $G_p^*(q-l)$ around q, followed by retention of the terms up to the first-order derivatives. The result is

$$G_p(0,q) = G_{p,f}(0)\left[\frac{1}{2}\left\{G_p(0,q) + \frac{l}{2}\left.\frac{\partial G_p(z,q)}{\partial z}\right|_{z=0} - l\frac{\partial G_p(0,q)}{\partial q}\right\} + G_p^*(q) - l\frac{\partial G_p^*(q)}{\partial q}\right] \quad (10)$$

The range of validity of eq 10 is the same as that of eq 2.

Elimination of the terms containing $G_p^*(q)$ from eq 10 using eq 9 results in eq 11, which serves as the surface−boundary condition for eq 2.

$$l\frac{\partial G_p(0,q)}{\partial q} = \left(1 + \frac{2G_{p,f}^*}{G_{p,f}(0)}\right)^{-1}\left[\frac{l}{2}\left.\frac{\partial G_p(z,q)}{\partial z}\right|_{z=0} + G_p(0,q)\left\{1 - \frac{2}{G_{p,f}(0)} + \frac{2G_{p,f}^*}{G_{p,f}(0)}\right\}\right] \quad (11)$$

The probability weight of an internal segment situated at distance q from either end of the complete chain (of contour length rl) is denoted by $g_p(z,q)$ and can be obtained from $G_p(z,q)$ using the inversion symmetry considerations.

$$g_p(z,q) = \frac{G_p(z,q)G_p(z,rl-q)}{G_{p,f}(z)} \quad (12)$$

In the same manner, we can obtained the surface phase analogue of eq 12 as

$$G_p^*(q) = \frac{G_p^*(q)G_p^*(rl-q)}{G_{p,f}^*} \quad (13)$$

The normalized volume fraction of polymer at location z, i.e. $\phi_p(z)/\phi_p^b$ can now be obtained by averaging $g_p(z,q)$ over the contour length of the chain.

$$\frac{\phi_p(z)}{\phi_p^b} = \frac{1}{rl}\int_0^{rl} g_p(z,q)\, dq \quad (14)$$

In the two-dimensional surface phase, concentrations of polymer and solvent are expressed as area fractions, ψ^*. Thus

$$\frac{\psi_p^*}{\phi_p^b} = \frac{1}{rl}\int_0^{rl} g_p^*(q)\, dq \quad (15)$$

It is possible to replace $g_p^*(q)$ in eq 15 by $g_p(0,q)$ using the following relation, which can be easily derived from eqs 9, 12, and 13:

$$g_p^*(q) = g_p(0,q)\frac{G_{p,f}^*}{G_{p,f}(0)} \quad (16)$$

The resulting form of eq 15 can be compared with eq 14 to obtain

$$\frac{\psi_p^*}{\phi_p(0)} = \frac{G_{p,f}^*}{G_{p,f}(0)} \quad (17)$$

Equation 17 expresses the equilibrium relationship between the bound and the unbound states of a polymer segment in terms of concentrations.

For the monomeric solvent (denoted by subscript s), the probability weight at location z, $G_s(z)$, can be expressed in terms of volume fraction, $\phi_s(z)$, as

$$G_s(z) = e^{-u_s(z)/kT} = \frac{\phi_s(z)}{\phi_s^b} \quad (18)$$

In a similar manner we can write

$$G_s^* = e^{-u^*_s/kT} = \frac{\psi_s^*}{\phi_s^b} \quad (19)$$

The following additional equations are obtained by applying the constraint that the volume and area fractions must sum to unity:

$$\phi_s(z) + \phi_p(z) = 1 \tag{20}$$

$$\phi_s^b + \phi_p^b = 1 \tag{21}$$

$$\psi_s^* + \psi_p^* = 1 \tag{22}$$

We write the self-consistent potential of a polymer segment or a solvent molecule as the sum of hard core (space filling) and interaction contributions,[14] the latter being based on the Flory−Huggins theory. Thus

$$u_s(z) = u^0(z) + \chi kT[\phi_p(z) - \phi_p^b] \tag{23}$$

$$u_p(z) = \frac{\bar{V}_p}{\bar{V}_s}\{u^0(z) + \chi kT[\phi_s(z) - \phi_s^b]\} \tag{24}$$

where $\bar{V}_p$ and $\bar{V}_s$ are the partial volumes of the polymer segment and solvent, respectively. The splitting the total potential in the manner outlined above is in accordance with the self-consistent field theories.[15] Both the hard core potential, u^0, and the parameter χ, which are molecular size dependent, are based here on the volume of the solvent molecule. The term $\bar{V}_p/\bar{V}_s$ in eq 24, therefore, corrects $u_p(z)$ for the difference between the sizes of the polymer segment and the solvent molecule.

Eliminating $u^0(z)$ from eqs 23 and 24 and replacing $u_s(z)/kT$ by $-\ln[(1 - \phi_p(z))/(1 - \phi_p^b)]$ in view of eqs 18 and 20, we obtain the following expression for $u_p(z)$:

$$u_p(z) = -kT\frac{\bar{V}_p}{\bar{V}_s}\left[\ln\left\{\frac{1 - \phi_p(z)}{1 - \phi_p^b}\right\} + 2\chi\{\phi_p(z) - \phi_p^b\}\right] \tag{25}$$

The above equation can also be derived using the free energy expression of Helfand and Sapse[16] in the manner outlined by Evans.[17]

In the surface phase, the expressions analogous to eqs 23 and 24 are

$$u_s^* = u^{0*} + kT(\chi'\psi_p^* - \chi\phi_p^b) + \chi_s^* kT \tag{26}$$

$$u_p^* = \frac{\bar{a}_p}{\bar{a}_s}\{u^{0*} + kT[\chi'\psi_s^* - \chi\phi_s^b] + \chi_p^* kT\} \tag{27}$$

where $\bar{a}_s$ and $\bar{a}_p$ refer to the partial areas, in the surface phase, of the polymer segment and the solvent molecule, respectively, while χ_s^* and χ_p^* are the corresponding energy parameters quantifying interactions with the solid phase. χ_i^* (i = s, p) is defined as the contact energy of species i when it occupies area $\bar{a}_s$ in the surface phase. The ratio $\bar{a}_p/\bar{a}_s$ in eq 27 corrects the energy for the fact that one polymer segment occupies area $\bar{a}_p$ of the surface.

In eqs 26 and 27, the energy of contact between a solvent molecule and a polymer segment in the surface phase is expressed using the modified Flory−Huggins parameter, χ', which is based on the area of contact between the two species. The value of χ' may be different from that of χ owing to a different pattern of molecular packing in the surface phase and alteration in the energy field due to the presence of the solid phase.

Following the procedure similar to that used in the derivation of eq 25, we obtain the expression for u_p^* from eqs 26, 27 and 19 as

$$-\frac{u_p^*}{kT} = \frac{\bar{a}_p}{\bar{a}_s}\left[\ln\left\{\frac{1 - \psi_p^*}{1 - \phi_p^b}\right\} + 2\{\chi'\psi_p^* - \chi\phi_p^b\}\right] + \chi^* \tag{28}$$

where

$$\chi^* = \frac{\bar{a}_p}{\bar{a}_s}(\chi_s^* - \chi_p^* + \chi - \chi') \tag{29}$$

χ^* may be called the adsorption energy parameter. It quantifies the strength of adsorption of the polymer species relative to the solvent species.

To simultaneously satisfy the volume and the area filling constraints, it is necessary to have

$$\frac{\bar{a}_p}{\bar{a}_s} = \frac{\bar{V}_p}{\bar{V}_s} \tag{30}$$

Substituting for $u_p(z)$ and u_p^* from eqs 25 and 28 into eqs 3 and 8 respectively, we get

$$G_{p,f}(z) = \left[\frac{1 - \phi_p(z)}{1 - \phi_p^b}\right]^{(\bar{V}_p/\bar{V}_s)} \exp\left\{2\chi\frac{\bar{V}_p}{\bar{V}_s}[\phi_p(z) - \phi_p^b]\right\} \tag{31}$$

$$G_{p,f}^* = \left[\frac{1 - \psi_p^*}{1 - \phi_p^b}\right]^{(\bar{V}_p/\bar{V}_s)} \exp\left\{\frac{2\bar{V}_p}{\bar{V}_s}(\chi'\psi_p^* - \chi\phi_p^b) + \chi^*\right\} \tag{32}$$

These two equations form the closure conditions for self-consistency since they relate the "input" variables $G_{p,f}(z)$ and $G_{p,f}^*$ of the connectivity equations, with its "output" variables $\phi_p(z)$ and ψ_p^*.

The connectivity shown in eq 2 along with initial condition (eq 4) and boundary conditions (eqs 5 and 11) can be solved in conjunction with eqs 31 and 32 to yield $G_p(z,q)$. The volume fraction, $\phi_p(z)$, and surface area fraction, ψ_p^*, can then be obtained using eqs 12−17. Since eqs 31 and 32 require a priori knowledge of $\phi_p(z)$ and ψ_p^*, the solution of the entire set of equations must be obtained in an iterative manner. The details of the solution procedure are described in the next section.

There are some quantities of interest which can be derived from the model as follows. The segmental volume fraction is given by the product of the segmental probability weight and its volume fraction in the in the bulk, i.e.

$$\phi_p(z,q) = g_p(z,q)\left\{\frac{\phi_p^b}{r}\right\} \tag{33}$$

The segmental area fraction in the surface phase can be obtained in analogous manner as

$$\psi_p^*(q) = g_p^*(q)\left\{\frac{\phi_p^b}{r}\right\} \tag{34}$$

The normalized segmental concentration in the solution phase may be defined as

$$f_q(z) = \frac{r\phi_p(z,q)}{\phi_p(z)} \tag{35}$$

where the term $\phi_p(z)/r$, which represents the average segmental volume fraction, is used as the normalizing factor. The corresponding normalized segmental concentration in the surface phase is

$$f_q^* = \frac{r\psi_p^*(q)}{\psi_p^*} \tag{36}$$

The adsorbed mass of the polymer per unit surface area is given by

$$\Gamma = \frac{M_p}{N_{av}}\left[\frac{1}{\bar{V}_p}\int_0^\infty \{\phi_p(z) - \phi_{p,f}(z)\}\, dz + \frac{\psi_p^*}{\bar{a}_p}\right] \tag{37}$$

where M_p refers to the molecular weight of polymer segment and N_{av} to the Avogadro number. $\phi_{p,f}(z)$ is the volume fraction of the unadsorbed (or free) chains, i.e., those chains which do not have even a single segment in the surface phase. It is computed using the procedure outlined by Scheutjens and Fleer.[18] We define a normalized adsorbed amount, $\hat{\Gamma}$, as

$$\hat{\Gamma} = \frac{\Gamma \bar{V}_p N_{av}}{l M_p}$$

$$= \frac{1}{l}\int_0^\infty [\phi_p(z) - \phi_{p,f}(z)]\, dz + \frac{\psi_p^*}{R} \tag{38}$$

The quantity $\hat{\Gamma}$ can be viewed as the thickness (expressed as multiples of l) of a hypothetical adsorbed layer, having the same adsorbed mass per unit area but is compacted by excluding the solvent. The contribution ψ_p^*/R, to the adsorbed amount, is due to the surface phase, the quantity R being defined as

$$R = \frac{\bar{a}_p}{(\bar{V}_p/l)} \tag{39}$$

This quantity can be viewed as the ratio of the actual area occupied by a polymer chain segment in the surface phase to the area obtained by projecting the segment from the solution on to the surface. The magnitude R would depend on the surface density of the active sites on which the adsorption of polymer occurs. If the adsorption sites are sparsely spaced, the polymer segment tends to extend on the surface. This results in a higher value of R than when the adsorption sites are closely spaced.

The bound fraction, that is the fraction of adsorbed polymer present in the surface phase, can be obtained using the following expression:

$$p = \frac{1}{\hat{\Gamma}}\left(\frac{\psi_p^*}{R}\right) \tag{40}$$

Method of Solution

To facilitate numerical computation, the upper limit of z ($z = \infty$) was truncated to a finite value, δ. This is justified by the fact that the polymer concentration profile decays rapidly and attains a near-bulk value at a short distance from the adsorbing surface.

The connectivity, equation, eq 2, and its boundary conditions can be converted into a set of linear ordinary differential equations in the normalized variable $\hat{q}$ by discretising the normalized $\hat{z}$ domain. The normalized variables are defined as

$$\hat{q} = \frac{q}{rl} \quad \text{and} \quad z = \frac{z}{\delta} \tag{41}$$

The general form of the resulting set of equations, in the vector form, after incorporating the boundary conditions is

$$\vec{\mathbf{B}}\frac{d\vec{\mathbf{G}}_p}{d\hat{q}} = \vec{\mathbf{C}}\vec{\mathbf{G}}_p + \vec{\mathbf{d}} \tag{42}$$

where $\vec{\mathbf{G}}_p$ is the vector $\{G_p(\hat{z}_i,\hat{q}_i),\ i = 1, ..., N\}$, z_i being the ith mesh point (node) of the $\hat{z}$ domain and N the total number of mesh points.

The nature of the square matrixes $\vec{\mathbf{B}}$ and $\vec{\mathbf{C}}$ and vector $\vec{\mathbf{d}}$ depends on the numerical method used. However, the elements of these matrixes do not contain $\hat{q}$. Hence eq 42 is linear in $\vec{\mathbf{G}}_p$, with constant coefficients, and can be solved analytically using the following initial condition

$$\vec{\mathbf{G}}_p(\hat{q} = 0) = \vec{\mathbf{G}}_{p,f} \tag{43}$$

to obtain

$$\vec{\mathbf{G}}_p = \vec{\mathbf{U}}_e^{\Lambda\hat{q}}\vec{\mathbf{U}}^{-1}[\vec{\mathbf{G}}_{p,f} + \vec{\mathbf{C}}^{-1}\vec{\mathbf{d}}] - \vec{\mathbf{C}}^{-1}\vec{\mathbf{d}} \tag{44}$$

where $\vec{\Lambda}$ is the diagonal matrix of eigenvalues satisfying the generalized eigenvalue problem

$$\vec{\mathbf{C}}\vec{\mathbf{u}}_i = \lambda_i\vec{\mathbf{B}}\vec{\mathbf{u}}_i \tag{45}$$

in which $\vec{\mathbf{u}}_i$ is the eigenvector corresponding to the eigenvalue λ_i. $\vec{\mathbf{U}}$, in the equation, is the matrix having eigenvectors $\vec{\mathbf{u}}_i$ as its columns.

The accuracy of the solution (eq 44) strongly depends on the accuracy of the eigenvalues λ_i (which are the elements of matrix $\vec{\Lambda}$), because error in these values is magnified by the exponential term in the equation, the extent of magnification increasing with increase in the chain length. For an accurate solution, it is also necessary that the matrixes $\vec{\mathbf{U}}$ and $\vec{\mathbf{C}}$ are well conditioned, so that their inverses appearing in eq 44 are accurately computed. A good choice of the numerical technique for discretization of $\hat{z}$ is important from this point of view. Those techniques which yield $\vec{\mathbf{C}}$ as symmetric and $\vec{\mathbf{B}}$ as symmetric as well as positive definite matrixes, are desirable because this ensures real eigenvalues and eigenvectors of eq 45, which can be accurately computed using the technique available in the literature.[19] The required inverses of $\vec{\mathbf{U}}$ and $\vec{\mathbf{C}}$ can also be accurately obtained using the following equation:

$$\vec{\mathbf{U}}^{-1} = \vec{\mathbf{U}}^{\mathrm{T}}\vec{\mathbf{B}} \tag{46}$$

$$\vec{\mathbf{C}}^{-1} = \vec{\mathbf{U}}\vec{\Lambda}^{-1}\vec{\mathbf{U}}^{\mathrm{T}} \tag{47}$$

The finite element technique was chosen because it yields the matrixes $\vec{\mathbf{B}}$ and $\vec{\mathbf{C}}$ in the desired form. The domain of $z(0,1)$ was divided into M quadratic elements. Each element had three nodes, the central node being the midpoint of the element. The elements were numbered starting from the surface. The advantage of quadratic elements over linear elements is that they ensure continuity of the gradients of G_p at the junctions

of elements. This results in smooth profiles of G_p and the other variables derived from it.

In the finite element technique, $G_p(\hat{z},\hat{q})$ is expressed using the following interpolation formula:

$$G_p(\hat{z},\hat{q}) = \sum_{e=1}^{M}\sum_{i=1}^{3} N_i^e(\hat{z}) G_p^e(\hat{z}_i,\hat{q}) \tag{48}$$

Here $G_p^e(\hat{z}_i,\hat{q})$ denotes the value of G_p at node $\hat{z}_i$ of element e. The elemental interpolation functions $N_i^e(\hat{z})$ are of the quadratic form, and are expressed as

$$N_1^e(\hat{z}) = (1-\zeta^e)(1-2\zeta^e)I^e, \quad N_2^e(\hat{z}) = 4\zeta^e(1-\zeta^e)I^e, \quad \text{and } N_3^e(z) = \zeta^e(2\zeta^e-1)I^e \tag{49}$$

where I^e is the indicator function, the value of which is 1 inside element e, and 0 outside it. The term ζ^e denotes the local coordinate of a point inside element e and is related to $\hat{z}$ by the following equation:

$$\zeta^e = \frac{\hat{z} - \hat{z}_1{}^e}{\Delta_e} \tag{50}$$

Here, $\Delta_e(=\hat{z}_3{}^e - z_1{}^e)$ denotes the span of element e and $\hat{z}_i{}^e$ is the location of the ith internal node of element e ($i = 1, 2, 3$).

It is convenient to rewrite eq 48 in terms of the global interpolation functions, N_k ($k = 1, 2M+1$) as follows:

$$G_p(\hat{z},\hat{q}) = \sum_{k=1}^{2M+1} N_k(\hat{z}) G_p(\hat{z}_k,\hat{q}) \tag{51}$$

N_k are related to the elemental interpolation functions, N_i^e by the following set of equations.

$$N_k = \begin{cases} N_1{}^1 & k = 1 \\ N_1^{(k-1)/2} + N_1^{(k+1)/2} & k = 3, 5, \ldots, 2M-1 \\ N_2^{k/2} & k = 2, 4, \ldots, 2M \\ N_3^M & k = 2M+1 \end{cases} \tag{52}$$

A weak formulation of eq 2 can be obtained by using the modified Galerkin method as follows. The normalized form of eq 2 is multiplied, in turn, by each N_k ($k = 1, \ldots, 2M$) and integrated with respect to $\hat{z}$ (from 0 to 1), to obtain a set of $2M$ equations. The term involving the second derivative of $G_p(\hat{z},\hat{q})$, with respect to $\hat{z}$, is integrated by parts once. The resulting form of the equations is

$$\frac{1}{r}\frac{\partial}{\partial\hat{q}}\int_0^1 N_k(\hat{z}) G_p(\hat{z},\hat{q})\,d\hat{z} = -\delta_{k,1}\frac{\hat{l}^2}{6}\frac{\partial G_p(\hat{z})}{\partial\hat{z}}\bigg|_{\hat{z}=0} - \frac{\hat{l}^2}{6}\int_0^1 \frac{\partial N_k(\hat{z})}{\partial\hat{z}}\frac{\partial G_p(\hat{z},\hat{q})}{\partial\hat{z}}\,dz + \int_0^1\left[1 - \frac{1}{G_{p,f}(\hat{z})}\right]\times N_k(\hat{z}) G_p(\hat{z},\hat{q})\,dz \quad k = 1, 2, \ldots, 2M \tag{53}$$

where, $\hat{l}(= l/\delta)$ denotes the normalized statistical segment length. Note that the interpolation function corresponding to the terminal node ($k = 2M+1$) is omitted from eq 53, since the corresponding nodal value of G_p is known ($G_p(1,\hat{q}) = 1$).

The first derivative of $G_p(\hat{z},\hat{q})$ with respect to $\hat{z}$ at $\hat{z} = 0$ can be eliminated from eq 53 by means of eq 11 to yield

$$\frac{1}{r}\frac{\partial}{\partial\hat{q}}\int_0^1 N_k(\hat{z}) G_p(\hat{z},\hat{q})\,d\hat{z} + \frac{\hat{l}}{3r}\delta_{k,1}\left(1 + \frac{2G_{p,f}^*}{G_{p,f}(0)}\right)\frac{\partial G_p(0,\hat{q})}{\partial\hat{q}} = \frac{\hat{l}}{3}\delta_{k,1} G_p(0,\hat{q})\left[1 - \frac{2(1-G_{p,f}^*)}{G_{p,f}(0)}\right] - \frac{\hat{l}^2}{6}\int_0^1 \frac{\partial N_k(\hat{z})}{\partial\hat{z}}\frac{\partial G_p(\hat{z},\hat{q})}{\partial\hat{z}}\,dz + \int_0^1 N_k(\hat{z}) G_p(\hat{z},\hat{q})\left[1 - \frac{1}{G_{p,f}(\hat{z})}\right]d\hat{z} \tag{54}$$

The interpolation form of $G_p(\hat{z},\hat{q})$, from eq 51, can now be substituted into eq 54. The resulting equation can be rearranged and brought in the form of eq 42. The elements of matrices $\vec{\mathbf{B}}$, $\vec{\mathbf{C}}$, and vector $\vec{\mathbf{d}}$ in eq 42 are listed in the Appendix.

To obtain the expression for the volume fraction profile of the polymer from eq 44, we may proceed as follows. We can rewrite eq 44 as

$$G_p(\hat{z}_j,\hat{q}) = \sum_{m=1}^{2M} U_{jm} e^{\lambda_m\hat{q}} v_m - w_j \tag{55}$$

where

$$\vec{\mathbf{v}} = \vec{\mathbf{U}}^{-1}(\vec{\mathbf{G}}_{p,f} + \vec{\mathbf{C}}^{-1}\vec{\mathbf{d}}) \quad \text{and} \quad \vec{\mathbf{w}} = \vec{\mathbf{C}}^{-1}\vec{\mathbf{d}} \tag{56}$$

Using eq 55, we can modify eq 12 to obtain

$$g_p(z_j,\hat{q}) = \frac{1}{G_{p,f}(z_j)}\Big[\sum_{m=1}^{2M}\sum_{n=1}^{2M} U_{jm}U_{jn}v_m v_n e^{\{\lambda_m\hat{q} + \lambda_n(1-\hat{q})\}} - w_j\sum_{m=1}^{2M} U_{jm}v_m\{e^{\lambda_m q} + e^{\lambda_m(1-\hat{q})}\} + w_j{}^2\Big] \tag{57}$$

Substitution of $g_p(\hat{z}_j,\hat{q})$ from eq 57 into eq 14 and subsequent integration with respect to $\hat{q}$ result in the following expression for the nodal values of the polymer volume fraction.

$$\phi_p(\hat{z}_j) = \frac{\phi_p^b}{G_{p,f}(\hat{z}_j)}\left[\sum_{m=1}^{2M}\sum_{n=1,m}^{2M} U_{jm}U_{jn}v_m v_n\left(\frac{e^{\lambda_m} - e^{\lambda_n}}{\lambda_m - \lambda_n}\right) + \sum_{m=1}^{2M} U_{jm}^2 v_m^2 e^{\lambda m} - 2w_j\sum_{m=1}^{2M} U_{jm}v_m\left(\frac{e^{\lambda_m} - 1}{\lambda_m}\right) + w_j{}^2\right] \tag{58}$$

The iterative procedure begins with assigning guess values for $\vec{G}_{p,f}$ and $\vec{G}_{p,f}^*$. Using these values, the elements of matrices $\vec{\mathbf{B}}$, $\vec{\mathbf{C}}$, and vector $\vec{\mathbf{d}}$ are then computed. The next step is to compute the eigenvalues and the eigenvectors of the generalized eigenvalue problem (eq 45). This is followed by the calculation of $\phi_p(\hat{z}_j)$ ($j = 1, 2, \ldots, 2M$), using eq 58. The value of ψ_p^* is provided by eq 17. Residues (difference between the right and the left hand sides) of eqs 31 and 32 at the nodal points are then computed. The iterative procedure involves reduction of the sum squares of the residues within the specified

limit of tolerance by successive improvements in the guess values of $\vec{\mathbf{G}}_{p,f}$ and $G^*_{p,f}$.

The iterative procedure outlined above was carried out using the algorithm CONLES,[20] which provides an option to maintain the nonnegativity of iterated variables throughout the process of iteration. Using this option it was possible to eliminate extraneous solutions.

The initial set of guesses for $\vec{\mathbf{G}}_{p,f}$ and $G^*_{p,f}$ was found to be critical for the convergence of the iterative procedure. For low values of chain length ($r \leq 20$) and moderate bulk conditions ($\phi_p^b \leq 10^{-3}$) it is best to start with $G_{p,f}(z_i) = 1$ (for all z_i) and $G^*_{p,f} = e^{\chi^*}$. It is then possible to build the solution for a range of parameters by perturbing them, one at a time, in small steps and using the solution of the previous steps as the initial guess values for the next step.

Accuracy of the solution depends on three parameters, δ, the thickness of the interfacial region, α, the node-spacing parameter (defined below), and M, the number of elements. The value of δ should be large enough to contain the change caused by the surface. The required value of δ increases with increase in the chain length and decrease in the volume fraction of polymer in the bulk (ϕ_p^b). Two values of ϕ_p^b, viz. 1×10^{-6} and 1×10^{-3} were tested in these simulations. A single value of $\delta = 175l$ was found to be adequate up to a chain length of 10 000. For chain lengths in the range from 10 000 to 30 000, it was necessary to use $\delta = 250l$, in order to maintain the desired level of accuracy of the volume fraction profile (within 0.03%).

It is preferable to use unequal spacing of the elemental nodes, with smaller spacing near the surface. This facilitates accurate tracking of the sharp profiles near the surface, without using excessively large number of elements. The following formula was used to calculate the span Δ_i of element i.

$$\Delta_i = \frac{\alpha^{i-1}(\alpha - 1)}{\alpha^M - 1}, \quad i = 1, 2, ..., M \tag{59}$$

Here α is the node spacing parameter and represents the ratio of the spans of consecutive elements. The value of α can be varied between 1 and 2; the value of 1 implies equally spaced nodes. For a fixed value of M, an increase in the value of α results in more closely spaced nodes near the surface and allows accurate depiction of the profiles near the surface. On the other hand, a high value of α makes the last element very large. For example, for $\alpha = 2$, the last element has a span of 0.5δ. This obviously introduces inaccuracy in the tail profile, which extends well beyond 0.5δ. On the basis of these considerations, the value of $\alpha = 1.5$ was found to be optimal and was, therefore, selected.

With these values of α and δ, the adsorbed amount was found to be insensitive (up to four significant figures) to the number of elements beyond $M = 20$. This value of M was, therefore, used in the subsequent simulations.

Simulations were conducted on Digital personal workstation-Alpha 433 au. For the parameters specified in Figure 2, it required a CPU time of 323 s to sweep through the entire range of chain lengths, starting from $r = 10$ and ending in $r \approx 10\,000$. For each new step, the chain length was augmented by 5% of its previous value. The total of 140 steps were required. A polynomial extrapolation routine was used to update the guess values of $\vec{\mathbf{G}}_{p,f}$ and $G^*_{p,f}$ for the current step, using the results of the five previous steps.

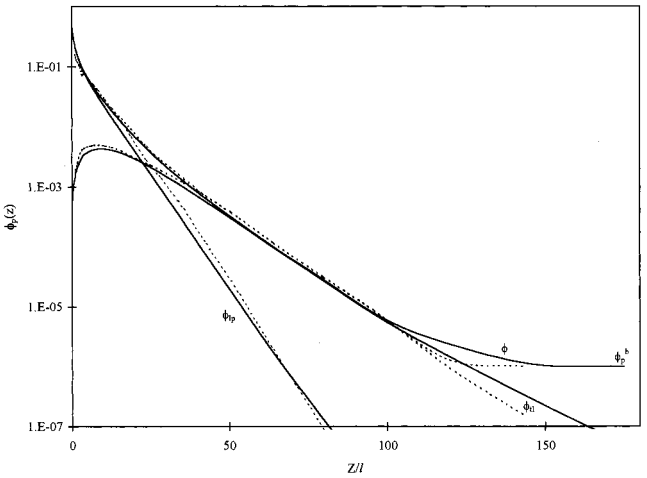

Figure 2. Segment volume fraction profile $\phi_p(z)$ and contribution from loops, ϕ_{lp}, and tails, ϕ_{tl}. The solid lines represent prediction of the present model and the dotted lines, that of SF model (data from Figure 5.2.2 of ref 15). Parameters common to both are as follows: $r = 10000$; $\chi^* = 1$; $\chi = 0.5$; $\phi_p^b = 10^{-6}$. The model specific parameters are as follows: lattice type-hexagonal (SF); $\bar{V}_s/\bar{V}_p = 1$; $R = 1$ (present model). The profile for the SF plot is obtained after contracting the z/l scale of the original SF plot by a factor of 0.816.

It is worthwhile to compare the present computational procedure with that based on the lattice model.[2] The latter involves determination of $r \times M$ segmental probabilities, M being the number of the lattice layers. This requires $r - 1$ successive multiplications of the tridiagonal matrix of order M, containing free segment probabilities. The computational intensiveness of the procedure lies in this matrix multiplication step. Since the matrix is nonsymmetric, it is not amenable to eigenvalue analysis and the straight forward repeated multiplication procedure has to be employed. Hence the computing time increases with increase in the chain length. Scheutjens and Fleer[2] have observed that the overall computing time increases roughly quadraticly with increase in r. With the present procedure, the segmental probabilities can be directly calculated using eq 57, which only requires the solution of the generalized eigenvalue problem represented by eq 45. Herein lies the computational advantage of the present procedure.

Results and Discussions

In this section, we compare the trends predicted by our model with those based on the Scheutjens and Fleer (SF) model.[2] The SF model, despite being lattice based, has been chosen for comparison because it provides the most detailed information about the structure of the adsorbed layer.

Figure 2 compares, on a semilogarithmic scale, the volume fraction profile of polymer (ϕ_p), the loop contribution (ϕ_{lp}), and the tail contribution (ϕ_{tl}) in the adsorbed layer as predicted by the two models. The prediction of the present model are shown by the solid lines while those of the SF model by dotted lines. Scheutjens and Fleer have used the hexagonal of the lattice in their simulation. The correspondence between the statistical length (l) of continuum model and lattice

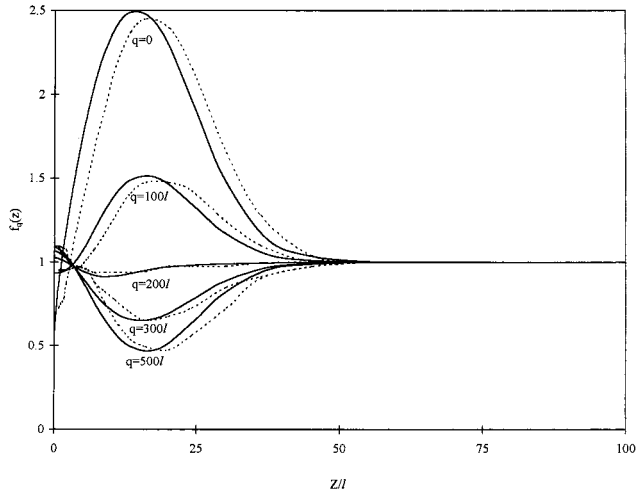

Figure 3. Comparison of the normalized segmental volume fraction profile, $f_q(z)$. The solid lines represent prediction of the present model and the dotted line, that of the SF model (data from Figure 5.2.7 C of ref 15). Parameters common to both are as follows: $r = 1000$, $\chi^* = 1$; $\chi = 0.5$; $\phi_p^b = 10^{-3}$. The model specific parameters are as follows: lattice type-hexagonal (SF); $\bar{V}_s/\bar{V}_p = 1$; $R = 1$ (present model). The profiles for the SF plot are obtained after contracting the z/l scale of the original SF plot by a factor of 0.816.

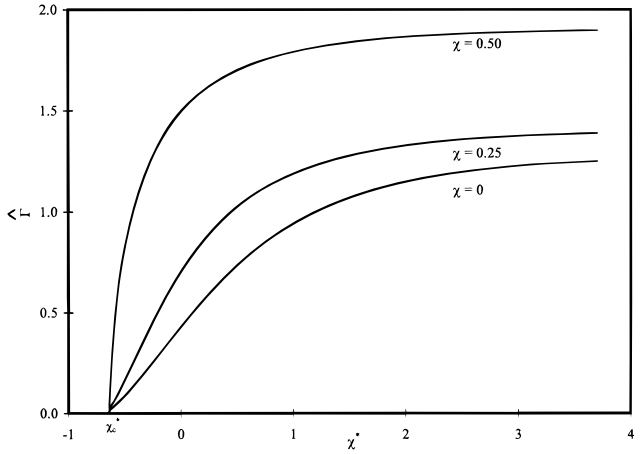

Figure 4. Variation of the normalized adsorbed amount, $\hat{\Gamma}$, with χ^*, at various values of χ. Parameters: $r = 10000$; $\phi_p^b = 10^{-6}$; $\bar{V}_s/\bar{V}_p = 1$; $R = 1$.

dimension (l_l) can be obtained by the following equation[21]

$$l_l = \frac{l}{\sqrt{6\lambda_l}} \tag{60}$$

where λ_l is the lattice parameter, the value of which is $^1/_4$ for hexagonal lattice. Using the value of λ_l, we find that l_l is 0.816l. This implies that for a correct comparison, the z/l scale for SF plot should be contracted by a factor of 0.816. Figure 2, therefore, shows the SF plots after the necessary contraction of the scale. The two sets of the plots are in good agreement.

Figure 3 compares the normalized segmental profiles, $f_q(z)$ (see eq 35), of the two models for different values of q. In this case also, we have shown SF profiles after contraction of the z/l scale by a factor of 0.816. We see again that the two profiles agree well.

In Figure 4, variation of the adsorbed amount with χ^* is highlighted for a very long polymer chain (r = 10000). This chain can be viewed as a approximately infinitely long chain. At high values of χ^*, the adsorbed amount is seen to reach a plateau. This is in accordance with the SF theory. The plot also indicates the critical value of χ^* ($=\chi_c^*$) at which the adsorbed amount reaches zero value. The value of χ_c^* is seen to be negative. The exact estimate of χ_c^* can be obtained using eqs 11 and 32. For an infinitely long chains, $G_p(0,q)$ is independent of q and the left-hand side term in eq 11 is zero. Second, since the surface has no influence on the composition of the solution phase at the critical point, the solution attains a uniform concentration, ϕ_p^b, right down to $z = 0$. This implies the gradient of $G_p(z,q)$ with respect to z is zero and also $G_p(0,q) = G_{p,f}(0) = 1$ in eq 11. Under these conditions, eq 11 yields $G_{p,f}^* = 0.5$. Substituting this value of $G_{p,f}^*$ in eq 32 and also noting that $\psi_p^* = 0$, we obtain the following expression for χ_c^*:

$$\chi_c^* = -\ln(2) + \frac{\bar{V}_p}{\bar{V}_s}[\ln\{1 - \phi_p^b\} + 2\chi\phi_p^b] \tag{61}$$

For a dilute solution ($\phi_p^b \ll 1$), eq 61 simplifies to

$$\chi_c^* = -\ln(2) \tag{62}$$

A deeper insight into this result can be obtained by comparing the connectivity equation at the surface, (eq 6) with its counterpart (eq 1) at a point not constrained by the surface. Since at $\chi^* = \chi_c^*$, both $G_p(z_s,q - l)$ and $G_p(z_h,q - l)$ are equal to 1, the value of the surface integral in eq 1 reduces to 1 and that in eq 6 reduces to $^1/_2$. This implies that any segment, which is connected a segment in the surface phase, would suffer a loss of probability weight of magnitude $^1/_2$. This loss must be compensated by the term $G_p^*(q - l)$ in eq 6, to bring $G_p(0,q)$ up to 1. This leads to $G_p^*(q - l) = 1/2 = e^{\chi_c^*}$ and hence $\chi_c^* = -\ln(2)$.

The above result differs from that of the SF theory, which predicts a positive value of χ_c^*. SF theory postulates that a segment at $z = 0$ (which corresponds to the first layer in the lattice theory), can exist only in the bound state. If an additional unbound state is allowed for a segment at $z = 0$, present theory provides an extra degree of freedom to the segment and hence makes the surface entropically more favorable than in the SF theory. Consequently, the present model predicts a lower value of χ_c^*.

Experimental Validation

The model was validated using three sets of experimental data reported in the literature. All these pertain to adsorption of polystyrene (PS) from cyclohexane (CH) at a temperature of 308 K. Kawaguchi et al.[22] and Vander Linden and van Leemput[23] have used silica, while Takahashi et al.[24] have used chrome as the substrate. Experimental conditions used by these authors are listed in Figure 5. For the PS−CH system, the following relations can be derived:[12] $l = 11.064l_b$; $r = 1.738 \times 10^{-3}M_w$; $\hat{\Gamma} = 6.482 \times 10^6\Gamma$. l_b is the average length of the C−C bond in the polymer backbone, M_w is the molecular weight of the polymer, and Γ is the adsorbed amount measured in g/cm^2. The volume ratio, $\bar{V}_p/\bar{V}_s$ (=5.069), is the product of two quantities, the ratio of the molar volume of repeat unit in polystyrene to that

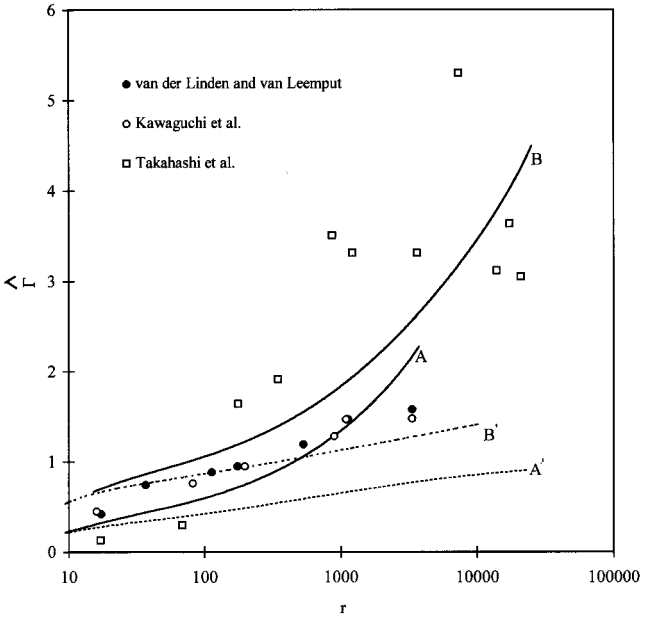

Figure 5. Variation of the adsorbed amount with chain length for adsorption of polystyrene from cyclohexane at $T = 308$ K. The squares denote experimental data for adsorption on chrome (Takahashi et al.[24]), while the circles denote adsorption on silica (van der Linden and van Leemput[23] and Kawaguchi et al.[22]). Bulk concentrations of the polymer used for the experiments were 3 g/L by Takahashi et al. and 2 mg/g by Kawaguchi et al. and van der Linden and van Leemput. Curves A and A′ are predictions of the present model for PS−CH on silica ($\chi_0 = 0.498$, $\chi^* = 1.9$, $\phi_p^b = 1.557 \times 10^{-3}$, $R = 3.3$). Curves B and B′ are the predictions for PS−CH on chrome ($\chi_0 = 0.498$, $\chi^* = 1.5$, $\phi_p^b = 2.857 \times 10^{-3}$, $R = 1$). In curves A and B variation of χ with volume fraction is taken into account ($p_1 = 0.6$ and $p_2 = 0$ in eq 63), while in A′ and B′ it is ignored ($p_1 = 0$, $p_2 = 0$).

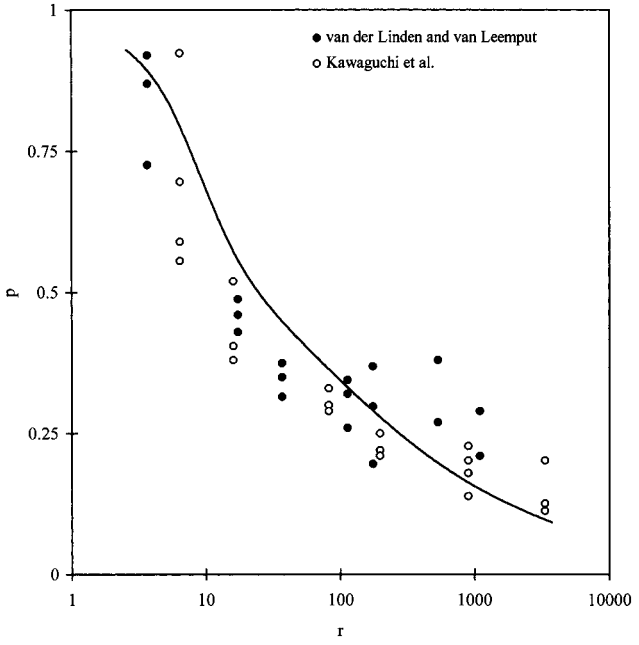

Figure 6. Variation of bound fraction with chain length for adsorption of polystyrene from cyclohexane on silica at $T = 308$ K (experimental data of van der Linden and van Leemput[23] and Kawaguchi et al.[22]). The curve represents prediction of the present model. The parameters used are the same as those for curve A of Figure 5.

of cyclohexane (=0.9163) and the ratio $l/2l_b$ (=5.532), which represents the number of repeat units per statistical segment of polystyrene.

The Flory−Huggins parameter, χ, is a strong function of the volume fraction of polymer, ϕ_p. Since ϕ_p varies widely in the interfacial region, its effect on χ cannot be ignored. We used the following correlation suggested by Kamide et al.[25,26]

$$\chi = \chi_0(1 + p_1\phi_p + p_2\phi_p^2)\left(1 + \frac{k'}{r}\right) \qquad (63)$$

where, χ_0 represents the Flory−Huggins parameter in the limits of zero polymer concentration and infinite chain length, and is given by the following equation

$$\chi_0 = \frac{1}{2} - \omega_0\left(1 - \frac{T_\theta}{T}\right) \qquad (64)$$

in which T_θ is the Flory temperature. The value of T_θ and the other parameters of eqs 63 and 64 for PS−CH system are reported by Kamide and Matsuda[27] as $T_\theta = 306.4$ K, $p_1 = 0.6$, $p_2 = 0$, and $\omega_0 = 0.35$. The value of k', which is a temperature-dependent parameter, is −0.8 at 308 K.[25,26] Using eq 63, the value of χ_0 is calculated as 0.498.

The other model parameters are χ^* and R. The values of χ^* used were those reported in the literature (1.9 for adsorption on silica[15] and 1.5 for chrome[28]). The area occupancy parameter, R, is expected to have a stronger effect on the bound fraction, than on the adsorbed amount. Consequently, the value of R for silica (for which the bound fraction data are reported), was chosen as 3.33, which was the best fit value for the bound fraction data. A high value of R for silica indicates that its active surface sites are sparsely placed. In absence of the bound fraction data for chrome, the value of R for this substrate was chosen as 1.

Figure 5 compares the simulation results with the experimental data on adsorbed amount vs chain length. The corresponding comparison of with the bound fraction data is reported in Figure 6. The agreement between the two appears to be satisfactory. We especially note strong increasing trend of the curves A and B in Figure 5, which can be attributed to the effect of ϕ_p on χ given by eq 63. To illustrate the importance of this effect, we re-simulated the model, with $p_1 = p_2 = 0$ in eq 63. The results are represented by lines A′ and B′, which show a mildly increasing, linear trend. In the case of A and B, eq 63, acts as a 'feed-back loop". Thus a small increase in ϕ_p with r (as suggested by lines A′ and B′), gives rise to increase in χ (through eq 63), which results in a further increase in ϕ_p. This effect is especially strong because the system is in the vicinity of the Θ condition, where the volume fraction is very sensitive to χ.

Conclusions

The continuum model presented here provides detailed configurational statistics of adsorbed polymer chains, in contrast to other continuum models reported in the literature. In addition, the model offers a framework to determine the effect of surface characteristics on adsorption phenomena. This model incorporates the boundary constraints on chain configuration in a mathematically consistent manner. A consequence of this boundary condition is that the model predicts a negative

value which appears to be physically realistic. Other predictions are in accordance with those of Scheutjens and Fleer model. The model is a good representation of the experimental data, provided the effect of the polymer volume fraction on the Flory−Huggins parameter is accounted for. The present model offers a significant computational advantage over lattice-based models for long chains.

Acknowledgment. The authors would like to thank (i) Unilever Research India for providing sponsorship and computational facilities and (ii) Dr. S. J. Suresh from Unilever Research India for valuable suggestions.

Appendix: Elements of Matrices $\vec{\mathbf{B}}$, $\vec{\mathbf{C}}$ and Vector $\vec{\mathbf{d}}$

First, we define the following matrices.

$$\mathbf{P}_{ij} = \frac{1}{\Delta_e}\int_{\Delta_c} N_i^e(\hat{z}) N_j^e(\hat{z})\, \mathrm{d}\hat{z} \tag{A.1}$$

$$\mathbf{Q}_{ij} = \Delta_e \int_{\Delta_e} \frac{\partial N_i^e(\hat{z})}{\partial \hat{z}} \frac{\partial N_j^e(\hat{z})}{\partial \hat{z}}\, \mathrm{d}\hat{z} \tag{A.2}$$

$$\mathbf{R}_{ijk} = \frac{1}{\Delta_e}\int_{\Delta_e} N_i^e(\hat{z}) N_j^e(\hat{z}) N_k^e(\hat{z})\, \mathrm{d}\hat{z} \tag{A.3}$$

The matrices $\vec{\mathbf{P}}$ and $\vec{\mathbf{Q}}$ are square, symmetric matrixes of order 3, while $\vec{\mathbf{R}}$ is a cubic, symmetric matrix of order 3.

The elements of the matrixes $\vec{\mathbf{B}}$ and $\vec{\mathbf{C}}$ and vector $\vec{\mathbf{d}}$ can now be written in terms of those of matrixes $\vec{\mathbf{P}}$, $\vec{\mathbf{Q}}$, and $\vec{\mathbf{R}}$ and the nodal values of $G_{\mathrm{p,f}}$. Thus

Elements of matrix $\vec{\mathbf{B}}$:

$$B_{11} = \frac{1}{r}\left[\Delta_1 P_{11} + \frac{\hat{l}}{3}\left(1 + \frac{2G^*_{\mathrm{p,f}}}{G_{\mathrm{p,f}}(0)}\right)\right] \tag{A.4}$$

$$B_{2j,2j} = \frac{\Delta_j}{r} P_{22} \quad j = 1, 2, ..., M \tag{A.5}$$

$$B_{2,j-1,2j-1} = \frac{1}{r}[\Delta_j P_{11} + \Delta_{j-1} P_{33}] \quad j = 2, 3, ..., M \tag{A.6}$$

$$B_{2j-1,2j} = B_{2j,2j-1} = \frac{\Delta_j}{r} P_{12} \quad j = 1, 2, ..., M \tag{A.7}$$

$$B_{2j-1,2j+1} = B_{2j+1,2j-1} = \frac{\Delta_j}{r} P_{13} \quad j = 1, 2, ..., M - 1 \tag{A.8}$$

$$B_{2j,2j+1} = B_{2j+1,2j} = \frac{\Delta_j}{r} P_{23} \quad j = 1, 2, ..., M - 1 \tag{A.9}$$

The rest of the elements of matrix $\vec{\mathbf{B}}$ are zero. $\vec{\mathbf{B}}$ is a $2M \times 2M$ symmetric, block-pentadiagonal, and positive definite matrix.

Elements of matrix $\vec{\mathbf{C}}$:

$$C_{11} = \frac{\hat{l}}{3}\left[1 - \frac{2}{G_{\mathrm{p,f}}(0)}(1 - G^*_{\mathrm{p,f}})\right] - \frac{\hat{l}^2 Q_{11}}{6\Delta_1} + \Delta_1 \sum_{k=1}^{3} R_{11k}\left(1 - \frac{1}{G_{\mathrm{p,f}}(\hat{z}_k)}\right) \tag{A.10}$$

$$C_{2j,2j} = -\left[\frac{\hat{l}^2 Q_{22}}{6\Delta_j} - \Delta_j \sum_{k=1}^{3} R_{22k}\left(1 - \frac{1}{G_{\mathrm{p,f}}(\hat{z}_{2j+k-2})}\right)\right] \quad j = 1, 2, ..., M - 1 \tag{A.11}$$

$$C_{2j-1,2j-1} = -\left[\frac{\hat{l}^2}{6}\left(\frac{Q_{11}}{\Delta_j} + \frac{Q_{33}}{\Delta_{j-1}}\right) - \sum_{k=1}^{3}\left\{\Delta_j R_{11k}\left(1 - \frac{1}{G_{\mathrm{p,f}}(\hat{z}_{2j+k-2})}\right) + \Delta_{j-1} R_{33k}\left(1 - \frac{1}{G_{\mathrm{p,f}}(\hat{z}_{2j+k-4})}\right)\right\}\right] \quad j = 2, 3, ..., M - 1 \tag{A.12}$$

$$C_{2j-1,2j} = C_{2j,2j-1} = -\left[\frac{\hat{l}^2 Q_{12}}{6\Delta_j} - \Delta_j \sum_{k=1}^{3} R_{12k}\left(1 - \frac{1}{G_{\mathrm{p,f}}(\hat{z}_{2j+k-2})}\right)\right] \quad j = 1, 2, ..., M - 1 \tag{A.13}$$

$$C_{2j-1,2j+1} = C_{2j+1,2j-1} = -\left[\frac{\hat{l}^2 Q_{13}}{6\Delta_j} - \Delta_j \sum_{k=1}^{3} R_{13k}\left(1 - \frac{1}{G_{\mathrm{p,f}}(\hat{z}_{2j+k-2})}\right)\right] \quad j = 1, 2, ..., M - 1 \tag{A.14}$$

$$C_{2j,2j+1} = C_{2j+1,2j} = -\left[\frac{\hat{l}^2 Q_{23}}{6\Delta_j} - \Delta_j \sum_{k=1}^{3} R_{23k}\left(1 - \frac{1}{G_{\mathrm{p,f}}(\hat{z}_{2j+k-2})}\right)\right] \quad j = 1, 2, ..., M - 1 \tag{A.15}$$

$$C_{2M-1,2M-1} = -\left[\frac{\hat{l}^2}{6}\left(\frac{Q_{11}}{\Delta_M} + \frac{Q_{33}}{\Delta_{M-1}}\right) - \sum_{k=1}^{2}\left\{\Delta_M R_{11k}\left(1 - \frac{1}{G_{\mathrm{p,f}}(\hat{z}_{2M+k-2})}\right) + \Delta_{M-1} R_{33k}\left(1 - \frac{1}{G_{\mathrm{p,f}}(\hat{z}_{2M+k-4})}\right)\right\}\right] \tag{A.16}$$

$$C_{2M-1,2M} = C_{2M,2M-1} = -\left[\frac{\hat{l}^2 Q_{12}}{6\Delta_M} - \Delta_M \sum_{k=1}^{2} R_{12k}\left(1 - \frac{1}{G_{\mathrm{p,f}}(\hat{z}_{2M+k-2})}\right)\right] \tag{A.17}$$

$$C_{2M,2M} = -\left[\frac{\hat{l}^2 Q_{22}}{6\Delta_M} - \Delta_M \sum_{k=1}^{2} R_{22k}\left(1 - \frac{1}{G_{\mathrm{p,f}}(z_{2M+k-2})}\right)\right] \tag{A.18}$$

The rest of the elements of matrix $\vec{\mathbf{C}}$ are zero. $\vec{\mathbf{C}}$ is a $2M \times 2M$ symmetric and block-pentadiagonal matrix.

Elements of vector $\vec{\mathbf{d}}$:

$$d_{2M-1} = -\left[\frac{\hat{l}^2 Q_{13}}{6\Delta_M} - \Delta_M \sum_{k=1}^{2} R_{13k}\left(1 - \frac{1}{G_{\mathrm{p,f}}(\hat{z}_{2M+k-2})}\right)\right] \tag{A.19}$$

$$d_{2M} = -\left[\frac{\hat{l}^2 Q_{23}}{6\Delta_M} - \Delta_M \sum_{k=1}^{2} R_{23k}\left(1 - \frac{1}{G_{\mathrm{p,f}}(\hat{z}_{2M+k-2})}\right)\right] \tag{A.20}$$

The the rest of the elements of $\vec{\mathbf{d}}$ are zero.

Nomenclature

$\bar{a}$: partial area occupied by a segment in the surface phase
$\mathbf{B}$, $\vec{\mathbf{C}}$, $\vec{\mathbf{d}}$: matrices defined by eq 42
f: normalized segmental concentration
g: probability weight an internal segment of a chain
G: probability weight of segment
k: Boltzmann constant
l: length of a statistical segment of polymer chain
l_b: bond length
M: number of finite elements, molecular weight
M_w: molecular weight of polymer chain
N: interpolation function
N_{av}: Avogadro number
p: bound fraction
q: distance from the chain end, measured along the contour of the chain
r: total number of statistical segments in a polymer chain
R: ratio of the actual area to the projected area of polymer segment
S: surface
T: absolute temperature
u: potential energy
$\vec{\mathbf{u}}$: eigenvector
$\mathbf{U}$: matrix of eigenvectors
V: partial volume of a segment in the solution
$\vec{\mathbf{v}}$, $\vec{\mathbf{w}}$: vectors as defined in eq 55
z: distance measured from the surface

Greek Letters

χ: Flory−Huggins parameter
χ^*: contact energy parameter
ζ: local coordinates of a finite element
α: ratio of spans of two successive elements
δ: width of the interfacial region
Δ: span of finite element
ϕ: volume fraction of species in the solution
ψ: area fraction of species in the surface phase
Γ: adsorbed amount per unit surface area
λ: eigenvalue
λ_j: lattice parameter
Λ: diagonal matrix of eigenvalues

Superscripts

b: bulk solution
e: finite element
*: surface phase
∧: normalized quantity

Subscripts

c: critical value
f: free segment
h: hemisphere
p: polymer
s: solvent, sphere

References and Notes

(1) Roe, R. J. *J. Chem. Phys.* **1974**, *60*, 4192.
(2) Scheutjens, J. M. H. M.; Fleer, G. J. *J. Phys. Chem.* **1979**, *83*, 1619; **1980**, *84*, 178.
(3) Helfand, E. *J. Chem. Phys.* **1975**, *62*, 999.
(4) Hong, K. M.; Noolandi, J. *Macromolecules* **1981**, *14*, 727.
(5) Ploehn, H. J.; Russel, W. B.; Hall, C. K. *Macromolecules* **1988**, *21*, 1075.
(6) Bohmer, M. R.; Evers, O. A.;Scheutjens, J. M. H. M. *Macromolecules* **1990**, *23*, 2288.
(7) de Gennes, P. G. *Scaling Concepts in Polymer Physics*; Cornell University Press: Ithaca, NY, 1979.
(8) de Gennes, P. G. *Macromolecules* **1981**, *14*, 1637.
(9) Jones, I. S.; Richmod, P. J. *J. Chem. Soc., Faraday Trans. 2* **1977**, *73*, 1062.
(10) Semenov, A. N.; Bonet-Avalos, J.; Johner, A.; Joanny, J. F. *Macromolecules* **1996**, *29*, 2179.
(11) Johner, A.; Bonet-Avalos, J.; van der Linden C. C.; Semenov, A. N.; Joanny, J. F. *Macromolecules* **1996**, *29*, 3629.
(12) Ploehn, H. J.; Russell, W. B. *Macromolecules* **1989**, *22*, 266.
(13) Helfand, E.; Tagami, Y. *J. Chem. Phys.* **1972**, *56*, 3592.
(14) Evers, O. A.; Scheutjens, J. M. H. M.; Fleer, G. J. *Macromolecules* **1990**, *23*, 5221.
(15) Fleer, G. J.; Cohen Stuart, M. A.; Scheutjens, J. M. H. M.; Cosgrove, T.; Vincent, B., *Polymers at Interfaces*; Chapman and Hall: London, 1993.
(16) Helfand, E.; Sapse, A. M. *J. Polym. Sci., Polym. Symp.* **1976**, *54*, 289.
(17) Evans, E. A. *Macromolecules* **1989**, *22*, 2277.
(18) Scheutjens, J. M. H. M.; Fleer, G. J. *J. Phys. Chem.* **1979**, *83*, 1619.
(19) Wilkinson, J. H.; Reinsch, C. *Handbook for Auto Comput., Vol II - Linear Algebra*; Springer-Verlag: New York, 1971.
(20) Shacham, M. *Int. J. Num. Methods Eng.* **1986**, *23*, 1455.
(21) Shull, K. R. *J. Chem. Phys.* **1991**, *94*, 5723.
(22) Kawaguchi, M.; Hayakawa, K.; Takahashi, A. *Polym. J.* **1980**, *12*, 265.
(23) Vander Linden, C.; van Leemput, R. *J. Colloid Interface Sci.* **1978**, *67*, 48.
(24) Takahashi, A.; Kawaguchi, M.; Hirota, H.; Kato, T. *Macromolecules* **1980**, *13*, 884.
(25) Kamide, K.; Miyazaki, Y. *Polym. J.* **1981**, *13*, 325.
(26) Kamide, K.; Abe, T.; Miyazaki, Y. *Polym. J.* **1982**, *14*, 355.
(27) Kamide, K.; Matsuda, S.; Dobashi, T.; Kaneko, M. *Polym. J.* **1984**, *16*, 839.
(28) Ploehn, H. J. *Macromolecules* **1994**, *27*, 1617.

MA980760I